nature climate change

LETTERS

PUBLISHED ONLINE: 29 APRIL 2012 | DOI: 10.1038/NCLIMATE1505

Impacts of wind farms on land surface temperature

Liming Zhou[1]*, Yuhong Tian[2], Somnath Baidya Roy[3], Chris Thorncroft[1], Lance F. Bosart[1] and Yuanlong Hu[4]

The wind industry in the United States has experienced a remarkably rapid expansion of capacity in recent years and this fast growth is expected to continue in the future[1–3]. While converting wind's kinetic energy into electricity, wind turbines modify surface–atmosphere exchanges and the transfer of energy, momentum, mass and moisture within the atmosphere[4–6]. These changes, if spatially large enough, may have noticeable impacts on local to regional weather and climate. Here we present observational evidence for such impacts based on analyses of satellite data for the period of 2003–2011 over a region in west-central Texas, where four of the world's largest wind farms are located[7]. Our results show a significant warming trend of up to 0.72 °C per decade, particularly at night-time, over wind farms relative to nearby non-wind-farm regions. We attribute this warming primarily to wind farms as its spatial pattern and magnitude couples very well with the geographic distribution of wind turbines.

Despite debates regarding the possible impacts of wind farms on regional to global scale weather and climate[8–12], modelling studies agree that they can significantly affect local scale meteorology[6,13–16] by increasing surface roughness, changing the stability of the atmospheric boundary layer (ABL) and enhancing turbulence in the rotor wakes[4–6]. However, these studies are based primarily on numerical simulations of regional and global models, which owing to lack of observations only crudely represent the effects of wind turbines by explicitly increasing either surface roughness length or turbulence kinetic energy. Evidently, more realistic model parameterizations should be developed and modelling results should be validated against the observations.

Although observed data on wind speed and turbulence in and around operational wind farms are readily available, information on other meteorological variables does not exist in the public domain. A recent study using the only available observed temperature data from an operational wind farm shows a warming effect at night and a cooling effect during the day[6]. However, the observed data are from only two meteorological towers for a period of 1.5 months. Hence more observational evidence, particularly on larger scales and for longer periods, is needed.

Satellites provide information on global spatial sampling at regular temporal intervals and thus have the potential to accurately monitor and detect the impacts of large wind farms with spatial detail. This study aims to search for observational evidence of such impacts from land surface temperature (LST) derived from Moderate Resolution Imaging Spectroradiometer (MODIS) with spatial resolutions finer than most wind farms and temporal resolutions covering both days and nights. LST is the radiometric temperature derived from surface emission and is closely related to land surface radiative properties[17].

Our study region (32.1°–32.9° N, 101°–99.8° W) is centred around 2,358 wind turbines (Supplementary Figs S1 and S2) in west-central Texas. We aggregate globally validated 1-km MODIS eight-day LST (ref. 18) and 16-day albedo[19] into anomalies at pixels of 0.01° (∼1.1 km) resolution from 2003 to 2011 in winter (December–January–February, DJF) and summer (June–July–August , JJA). For brevity, here we use the following acronyms to represent four different groups of pixels: ALL (all of the pixels); WFM (wind-farm pixels—those with at least one wind turbine); NWF (non-wind-farm pixels); and NNWF (nearby non-wind-farm pixels—those NWF pixels that are close to the wind farms). Besides possible impacts from wind farms, LST variability over the study region consists of two main components: first, temporal variability controlled primarily by regional or large-scale weather and climate conditions; and second, spatial variability at pixel level that is mostly related to changes in topography and land-cover types. So minimizing such variability (for example, removing the regional interannual variability introduced next and using the anomalies in our analysis) is the key to uncovering wind-farm impacts. Details about the study region and data processing are described in the Methods.

We first study the spatial patterns of LST changes and their spatial coupling with wind turbines by examining the LST differences between two given periods (referred to as method I). As the wind turbines in our study region were constructed in stages, with most built in 2005–2008 (Supplementary Fig. S2), we chose the first three years (2003–2005) of data to represent the case with the least impacts and the last three years (2009–2011) of data to represent the case with the most likely impacts. MODIS LST also contains the background regional interannual variability that is unrelated to wind farms (for example, overall the study region is warmer in 2011 than 2010; Fig. 1). For long-term time series of data, a low-pass filter or multiple-year averaging will reduce such a signal. Given the short period of the MODIS data, for each year we create a regional mean LST anomaly averaged from all pixels of the study region (one value in DJF and one in JJA per year; Fig. 1) and subtract this mean from the original anomalies. Doing so emphasizes the LST spatial variability on the pixel scale. For example, if a region is warmer in year y than year x but with different warming rates at different pixels, the LST change (y minus x) will show the warming everywhere, but after removing the regional mean warming rate, the spatial variability of the warming rate can be easily identified. Note that the resulting warming or cooling rate represents a change relative to the regional mean value.

[1]Department of Atmospheric and Environmental Sciences, University at Albany, State University of New York, 1400 Washington Avenue, Albany, New York 12222, USA, [2]I.M. Systems Group, Inc. at National Oceanic and Atmospheric Administration/National Environmental Satellite, Data, and Information Service/The Center for Satellite Applications and Research, 5200 Auth Road, Camp Springs, Maryland 20746, USA, [3]Department of Atmospheric Sciences, University of Illinois, 105 South Gregory Street, Urbana, Illinois 61801, USA, [4]Terra-Gen Power LLC, 11512 El Camino Real, San Diego, California 92130, USA. *e-mail: lzhou@albany.edu.

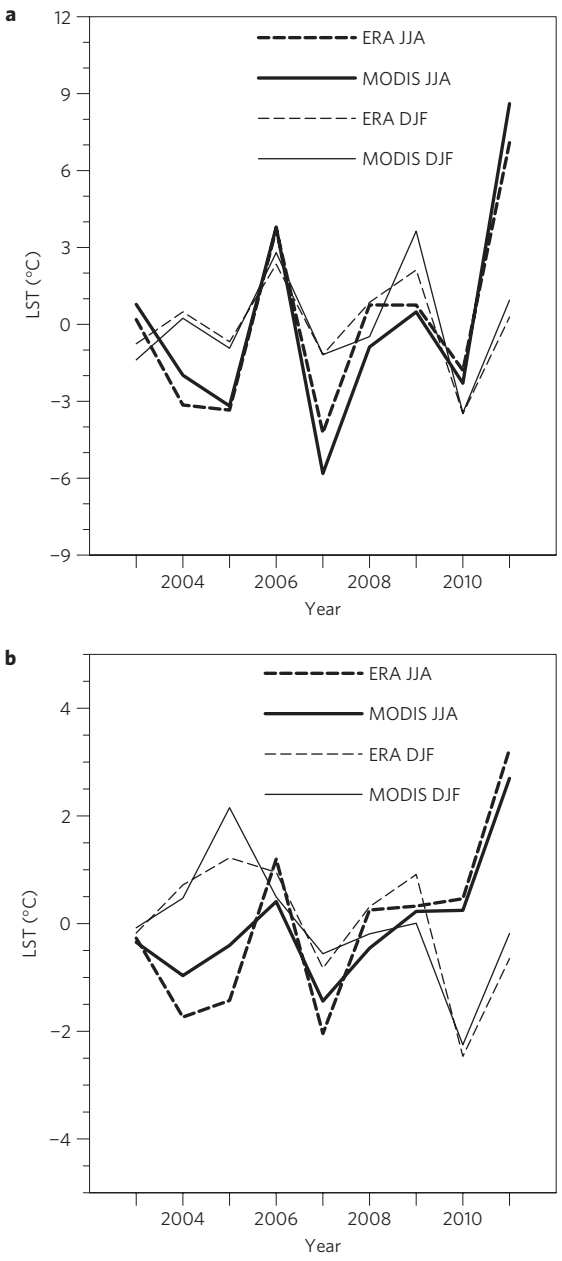

Figure 1 | Interannual variations of regional mean MODIS and ERA LST anomalies in DJF and JJA averaged over the study region for the period of 2003–2011. a, Daytime. **b**, Night-time. ERA LST data at 06:00 and 18:00 UT are chosen to represent the LST at night-time (local midnight) and daytime (local noon), which roughly correspond to the MODIS measurement times.

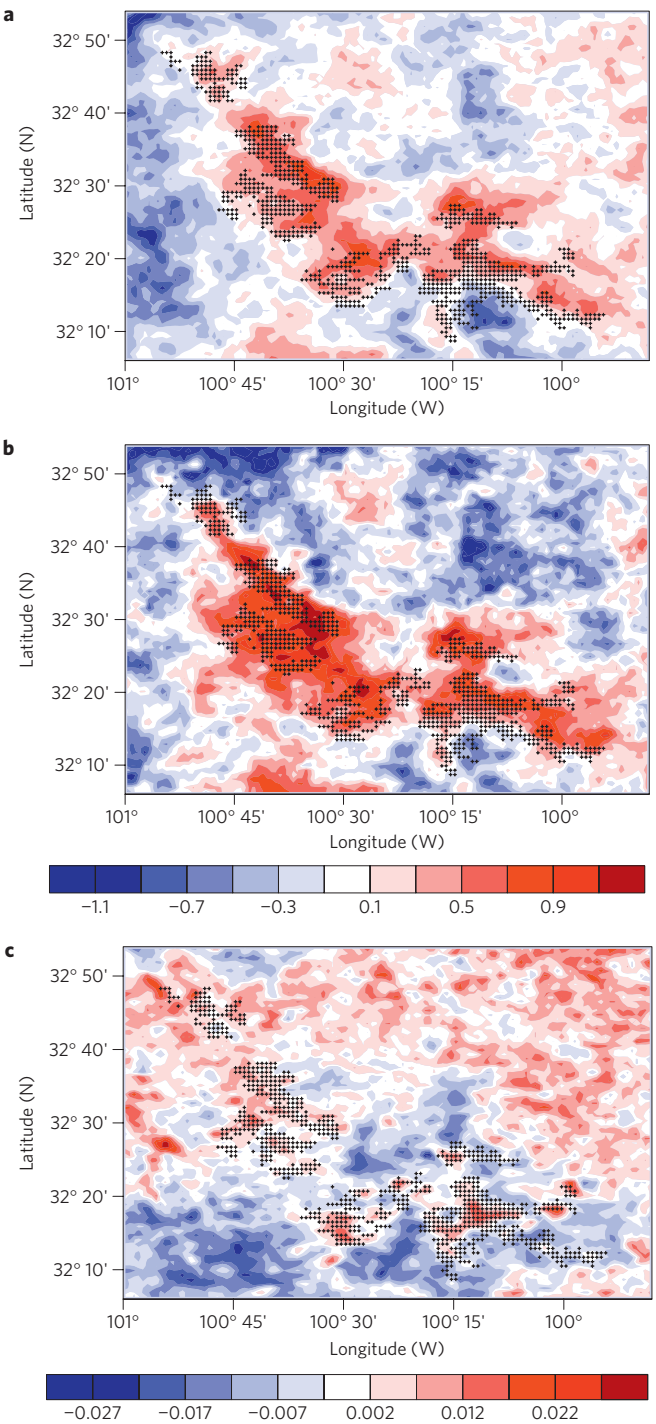

Figure 2 | MODIS JJA night-time LST and daytime shortwave-albedo differences for the period of 2003–2011. a,**b**, LST differences (°C): 2009–2011 minus 2003–2005 averages (**a**) and 2010 minus 2003 (**b**). **c**, Albedo differences (unitless): 2009–2011 minus 2003–2005 averages. Pixels with plus symbol have at least one wind turbine. Note that the regional interannual variability was removed from the original anomalies to emphasize the relative LST and albedo changes at pixel level (that is, method I).

Figure 2 shows the MODIS JJA night-time LST differences between the 2009–2011 and 2003–2005 averages (Fig. 2a) and between 2010 and 2003 (Fig. 2b). The latter is used to illustrate the LST change in two individual years. Note that 2003 and 2010 are chosen because their regional mean LSTs are similar in the study region (Fig. 1b). The WFM pixels are much warmer than their surrounding pixels and this warming is also observed at downwind pixels of wind turbines (the prevailing wind is from the south, Supplementary Fig. S3). Figure 2b exhibits similar features as Fig. 2a but with a larger magnitude, which is expected as it is from a single year whereas Fig. 2a is from a three-year average. The strong spatial coupling between the wind farms and the warming indicates causation. Similar features are also seen at night-time in DJF and also at local solar time ~22:30 and ~1:30 (Supplementary Figs S4–S7). The daytime LST shows a warming effect over most WFM pixels but their spatial coupling and the warming rate are much weaker than those at night-time (Supplementary Figs S4, S5).

We then quantify the impacts of wind farms on LST by examining the areal mean annual LST differences between WFM

versus NNWF pixels (WFM minus NNWF; Fig. 3; referred to as method II). This method has been extensively used to estimate urban-heat-island effects by comparing observed temperatures in urban stations with their nearby rural ones[20]. Unlike method I, method II does not explicitly remove the regional mean value but implicitly carries out the same function. Although the time series is short, we have identified statistically significant warming trends of 0.724 °C per decade ($p = 0.005$) in JJA and 0.458 °C per decade ($p = 0.001$) in DJF from 2003 to 2011 over the WFM pixels relative to the NNWF pixels. In contrast, the daytime LST shows strong interannual variations and no significant trends. We also try to define the WFM and NNWF in different ways and get similar results. On average, the warming is stronger and better coupled with wind farms during night-time than daytime and in JJA than DJF. Hence the warming trend is largest at night-time in JJA.

The diurnal cycle of LST results from the balance of the day/night contrast in solar heating and the radiative and dynamical cooling that responds to the temperature difference between the land surface and the atmosphere[21–23]. Its magnitude can be modified by three factors: incoming surface radiation; land surface properties (for example, elevation, land cover, albedo and emissivity); and ABL conditions near the surface. Given the small size of our study region, changes in radiative forcing are likely to be similar over the entire region. Local effects at pixel level owing to spatial variability in topography and land-cover types may introduce some LST variability as the wind turbines are generally built on topographic high ground, with an average elevation of 749.10 ± 21.38 m (21.38 is one standard deviation), but such effects have already been minimized by our approach (Supplementary Discussion and Figs S8–S17). So the warming trends over wind farms shown above should be mostly related to temporal changes in land surface properties and ABL conditions.

Some of the LST changes could result from changes in surface properties associated with the turbine footprint (that is, turbine blades, towers, access roads and so on) within wind farms. However, the footprint area occupies only a small percentage of the total land area of wind farms because substantial interturbine spacing is required to maximize turbine efficiency in capturing wind and also to avoid turbine wake effects[7,24]. Land surface properties can be also modified by changes in precipitation, clouds, soil moisture, vegetation and land cover/use (for example, irrigation, agricultural practice, urbanization and so on). As there are no surface observations of these variables available at ~1.1 km, MODIS data of vegetation greenness, albedo and land cover[25] are used to quantify possible changes in land surface properties. We find that such changes are small and cannot explain the warming effects over WFM pixels seen by MODIS (Supplementary Discussion, Tables S3–S4 and Figs S18–S22). There is a small increase in surface albedo and a small decrease in vegetation greenness over wind farms, possibly related to the turbine footprint. For example, the linear trend of albedo is +0.007 per decade ($p = 0.149$) in JJA and +0.013 per decade ($p = 0.021$) in DJF over WFM pixels relative to NNWF pixels (Fig. 3c), but this increase is too small to produce a notable daytime cooling[26] (Supplementary Figs S4, S5). Some large albedo changes observed over other NWF regions (Fig. 2c) are probably owing to changes in weather conditions (Fig. 1; Supplementary Discussion and Figs S19–S22).

Very probably the diurnal and seasonal variations in wind speed and the changes in near-surface ABL conditions owing to wind-farm operations are primarily responsible for the LST changes described above. The stronger wind speeds in JJA than DJF and at night-time than daytime (Supplementary Table S1) probably drive wind turbines to generate more electricity and turbulence and consequently result in the strongest warming effect at night-time in JJA. The nocturnal ABL is typically stable and much thinner than the daytime ABL and hence the turbine-enhanced vertical mixing produces a stronger night-time effect[27].

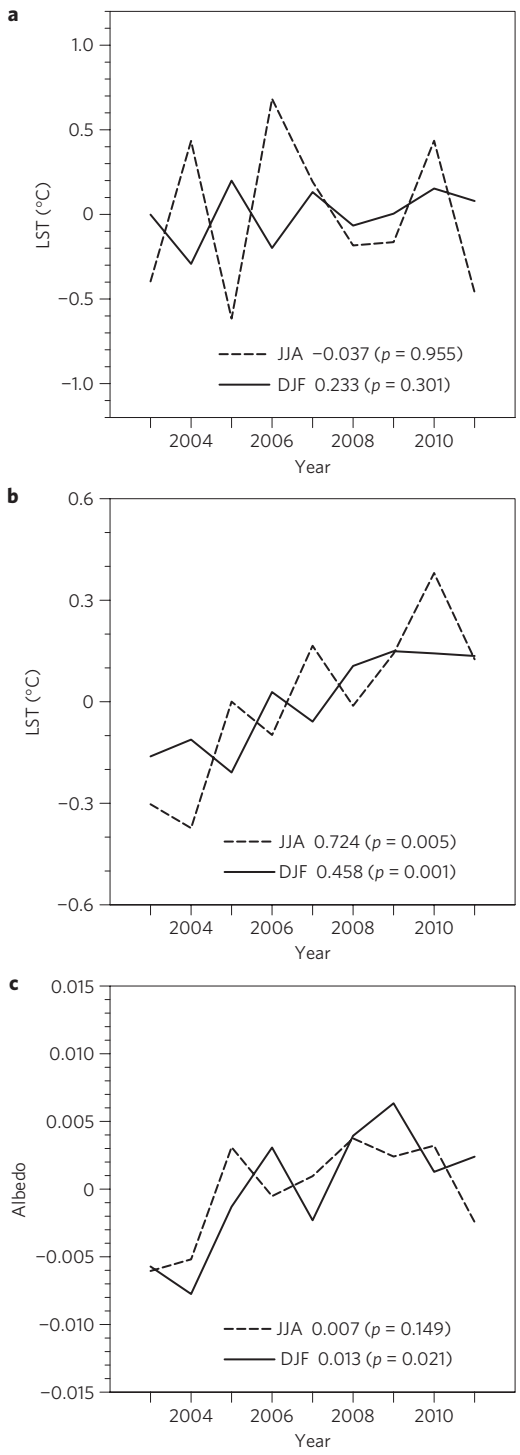

Figure 3 | Interannual variations in areal mean differences between WFM and NNWF pixels in DJF and JJA from MODIS for the period of 2003–2011. LST at daytime (**a**) and night-time (**b**) and shortwave albedo (unitless) at daytime (**c**). Linear trends (per decade) and significance levels (p values) estimated using least squares fitting are shown. The 95% confidence intervals for the linear trends are listed in Supplementary Table S2. WFM and NNWF pixels are defined in Supplementary Fig. S1.

One striking and contrasting feature of the ABL is the diurnal evolution with time about its depth and stability[28]. During daytime

the ABL is typically deep and unstable in nature, with cooler air overlying warmer air because of faster solar heating of the surface than the above air. It becomes much thinner and typically stable after sunset, with warmer air overlaying cooler air because of faster radiative cooling of the surface than the above air. Hence, it is expected that the enhanced vertical mixing in the wakes generated by wind-turbine rotors will create a warming effect at night-time and a cooling effect during the day.

Interestingly, our results also show a weak warming effect at daytime over wind farms (Supplementary Figs S4, S5). We speculate that the slow development of the daytime unstable and convective layer[28] might play a role. Furthermore, continuous conduction and convection help to create a well-mixed thick ABL in late afternoon, which exhibits a statically neutral profile where the vertical temperature gradients are approximately adiabatic. Hence, the effect of additional energy transport by turbulence in rotor wakes on LST is weak at best. Another possibility for the daytime warming could be the result of reduced convection in turbine wakes because vertical convective transport is the main mechanism by which heat is transported away from the surface.

We realize that the MODIS data do contain errors and noise[18,19]. Uncertainties also exist in locating wind turbines (for example, builders may relocate their turbine sites slightly from their original filing with the Federal Aviation Administration). Our use of spatial and temporal averaging should largely remove such errors and uncertainties, whose remaining residuals, if any, cannot accidentally create the strong spatial coupling between the warming and wind turbines shown above. Furthermore, as expected, we do see the increasing extent and magnitude of the spatial coupling with time between the warming trend and the increase of built wind turbines from 2000 to 2011 (Supplementary Fig. S12). In addition, the regional mean LST interannual variability of MODIS matches well with that of LST data from the European Centre for Medium-Range Weather Forecasts (ECMWF) Reanalysis (ERA LST; Fig. 1). Some discrepancies between the two LST data sets are expected, given their differences in spatial and temporal resolutions (for example, the timing in the diurnal cycle) and weather conditions (for example, the MODIS LST is retrieved from clear sky whereas the ERA LST is from all sky).

To the best of our knowledge, this research is the first in quantifying the impacts of large wind farms on surface temperature using satellite data. As this analysis is from a short period over a region with rapid growth of wind farms, our estimates should represent the wind-farm effects locally. However, given the present installed capacity and the projected installation across the world[1–3], this study draws attention to an important issue that requires further investigation. We need to better understand the system with observations and better describe and model the complex processes involved to predict how wind farms may affect future weather and climate.

Methods

Study region. Texas has the most installed wind-power capacity of any US state[1,2]. It has many big wind farms and west-central Texas, which represents the state's largest concentration of wind farms and the most active deployment and operations centre for wind energy, continues to experience rapid growth[7]. Here, we focus our study on a region (32.1°–32.9° N, 101°–99.8° W; Supplementary Fig. S1) in west-central Texas, with a total area of ~10,005 km^2 (112.8 km × 88.7 km).

Geographic location of wind turbines. We use the database of obstruction evaluation/airport airspace analysis at the FAA (https://oeaaa.faa.gov/oeaaa/external/portal.jsp) to locate wind farms. To promote air safety and the efficient use of the navigable airspace, the FAA requires any organization that plans to sponsor any construction or alterations that may affect navigable airspace to file a notice of proposed construction or alteration. It has the detailed record for each wind turbine built, altered or proposed in the period of 1988–2011. We downloaded all the records and identified wind turbines built in our study region based on their locations (latitude and longitude). The existence of these wind turbines can be also verified through Google Earth where each turbine is visible. In total, there are 2,358 wind turbines built as of 17 November 2011 (Supplementary Fig. S2).

MODIS data. We use the Collection 5 globally validated MODIS products of surface shortwave albedos, land cover and LST at 1 km resolution. MODIS instruments (Terra and Aqua) image the entire Earth's surface every one to two days, passing across the Equator at around local solar time ~10:30 (Terra) and ~13:30 (Aqua) during daytime and ~22:30 (Terra) and ~1:30 (Aqua) at night. As daily MODIS data have gaps and missing values, we downloaded from https://lpdaac.usgs.gov/get{_}dataeight-day average LST (ref. 18) of Terra (MOD11A2) and Aqua (MYD11A2) and 16-day albedos[19] (MCD43B3) and yearly land cover[25] (MCD12Q1) retrieved by combining the reflectance from Terra and Aqua. The MODIS data represent the best quality retrieval possible from clear-sky conditions over each composite period. They have been used extensively in a variety of areas and proved to be of high quality. For example, validation studies indicate that the errors of MODIS albedos are mostly <5% (ref. 29), the MODIS LST is generally better than 1 K (ref. 18) and the MODIS land cover is about 75% correctly classified[25]. For each pixel we aggregate the MODIS eight-day average LST into seasonal means (DJF and JJA) and calculate anomalies (referred to as seasonal anomalies) relative to the 2003–2011 climatology. The Terra and Aqua anomalies are then combined to produce daytime (averages of ~10:30 and ~13:30) and night-time (averages of ~22:30 and ~1:30) data. As the MODIS data are available in March 2000 for Terra and July 2002 for Aqua, there are in total nine years of the MODIS seasonal anomalies from 2003 to 2011. The MODIS albedos are processed similarly to create winter (DJF) and summer (JJA) anomalies. The MODIS annual land-cover map is available at 500 m resolution until 2009 and is reprojected into our study region using nearest-neighbour resampling. The MODIS data are achieved by tile (each tile represents a 10° by 10° grid cell) in the sinusoidal projection, which has a tilt angle of ~45° relative to local latitude/longitude. So the MODIS data were reprojected into pixels at 0.01° resolution. In total, there are 9,600 pixels (120 columns × 80 lines) over the study region.

Reanalysis data. We also use LST data from the ECMWF (ref. 30) and wind data from North American Regional Reanalysis (NARR; ref. 31) for the period of 2003–2011. Note that the NARR has a higher spatial resolution at 32 km but does not provide LST and so the ERA LST at 0.75° grid boxes is used. Monthly means of NARR winds at 30 m above the surface were downloaded from http://www.emc.ncep.noaa.gov/mmb/rreanl/. The climatological winds in DJF and JJA are created to help us identify downwind directions of wind farms and understand wind statistics (Supplementary Fig. S3 and Table S1). Monthly means of ERA LST were downloaded from http://data-portal.ecmwf.int/data/d/interim{_}mnth/. Like the MODIS LST, the ERA LST was averaged into seasonal means and anomalies and then reprojected into our study region at 0.01° resolution using bilinear interpolation. As the reanalysis is provided at 00:00, 06:00, 12:00 and 18:00 universal time (UT) in ERA and at 00:00, 03:00, 06:00, 09:00, 12:00, 18:00 and 21:00 UT in NARR, the reanalysis wind and LST at 06:00 and 12:00 UT are chosen to represent the data at night-time (local midnight) and daytime (local noon), which roughly correspond to the MODIS measurement times.

Received 2 February 2012; accepted 28 March 2012; published online 29 April 2012

References

1. American Wind Energy Association *AWEA 4th Quarter 2011 Public Market Report* (AWEA, 2012); available at http://awea.org/learnabout/publications/reports/upload/4Q-2011-AWEA-Public-Market-Report{_}1-31.pdf.
2. American Wind Energy Association *US Wind Energy Market Update* (AWEA, 2011); available at http://www.awea.org/learnabout/publications/factsheets/upload/Market-Update-Factsheet-Final_April-2011.pdf.
3. US Department of Energy *20% Wind by 2030* (USDOE, 2008); available at http://www1.eere.energy.gov/wind/pdfs/42864.pdf.
4. Knippertz, P., Ulbrich, U. & Speth, P. Changing cyclones and surface wind speeds over the North Atlantic and Europe in a transient GHG experiment. *Clim. Res.* **15,** 109–122 (2000).
5. Simmonds, I. & Keay, K. Surface fluxes of momentum and mechanical energy over the North Pacific and North Atlantic oceans. *Meteorol. Atmos. Phys.* **80,** 1–18 (2002).
6. Baidya, R. S. & Traiteur, J. J. Impacts of wind farms on surface air temperatures. *Proc. Natl Acad. Sci. USA* **107,** 17899–17904 (2010).
7. Combs, S. *The Energy Report 2008* (Texas Controller of Public Accounts, 2008); available at http://www.window.state.tx.us/specialrpt/energy/.
8. Keith, D. *et al.* The influence of large-scale wind power on global climate. *Proc. Natl Acad. Sci. USA* **101,** 16115–16120 (2004).
9. Kirk-Davidoff, D. B. & Keith, D. W. On the climate impact of surface roughness anomalies. *J. Atmos. Sci.* **65,** 2215–2234 (2008).
10. Sta Maria, M. R. V. & Jacobson, M. Z. Investigating the effect of large wind farms on energy in the atmosphere. *Energies* **2,** 816–838 (2009).
11. Barrie, D. & Kirk-Davidoff, D. Weather response to management of large wind turbine array. *Atmos. Chem. Phys.* **10,** 769–775 (2010).

12. Wang, C. & Prinn, R. J. Potential climatic impacts and reliability of very large-scale wind farms. *Atmos. Chem. Phys.* **10,** 2053–2061 (2010).
13. Fiedler, B. H. & Bukovsky, M. S. The effect of a giant wind farm on precipitation in a regional climate model. *Environ. Res. Lett.* **6,** 045101 (2011).
14. Baidya, R. S., Pacala, S. W. & Walko, R. L. Can large scale wind farms affect local meteorology? *J. Geophys. Res.* **109,** D19101 (2004).
15. Adams, A. S. & Keith, D. W. Wind energy and climate: Modeling the atmospheric impacts of wind energy turbines. *Eos Trans. AGU* **88** (Fall Meeting Suppl.), abstr. B44B-08 (2007).
16. Baidya, R. S. Simulating impacts of wind farms on local hydrometeorology. *J. Wind Eng. Ind. Aerodyn.* http://dx.doi.org/10.1016/j.jweia.2010.12.013(in the press).
17. Jin, M. & Dickinson, R. E. New observational evidence for global warming from satellite. *Geophys. Res. Lett.* **29,** 1400 (2002).
18. Wan, Z. New refinements and validation of the MODIS land surface temperature/emissivity products. *Remote Sens. Environ.* **112,** 59–74 (2008).
19. Schaaf, C. B. *et al.* First operational BRDF, albedo, and nadir reflectance products from MODIS. *Remote Sens. Environ.* **83,** 135–148 (2002).
20. Gallo, K. P. & Owen, T. K. Satellite-based adjustments for the urban heat island temperature bias. *J. Appl. Meteorol.* **36,** 1117–1132 (1997).
21. Dai, A., Trenberth, K. E. & Karl, T. R. Effects of clouds, soil moisture, precipitation, and water vapor on diurnal temperature range. *J. Clim.* **12,** 2451–2473 (1999).
22. Zhou, L. *et al.* Spatial patterns of diurnal temperature range trends on precipitation from 1950 to 2004. *Clim. Dynam.* **32,** 429–440 (2009).
23. Zhou, L., Dickinson, R. E., Tian, Y. & Vose, R. S. Impact of vegetation removal and soil aridation on diurnal temperature range in a semiarid region—application to the Sahel. *Proc. Natl Acad. Sci. USA* **104,** 17937–17942 (2007).
24. Denholm, P., Hand, M., Jackson, M. & Ong, S. *Land-use Requirements of Modern Wind Power Plants in the United States* Technical Report NREL/TP-6A2-45834 (2009); available at http://www.nrel.gov/docs/fy09osti/45834.pdf.
25. Friedl, M. A. *et al.* MODIS Collection 5 global land cover: Algorithm refinements and characterization of new datasets. *Remote Sens. Environ.* **114,** 168–182 (2010).
26. Zhou, L. *et al.* A sensitivity study of climate and energy balance simulations with use of satellite derived emissivity data over the northern Africa and the Arabian peninsula. *J. Geophys. Res.* **108,** 4795 (2003).
27. Eastman, J. L., Coughenour, M. B. & Pielke, R. A. The effects of CO_2 and landscape change using a coupled plant and meteorological model. *Glob. Change Biol.* **7,** 797–815 (2001).
28. Stull, R. B. *An Introduction to Boundary Layer Meteorology* 9–19 (Springer, 2009).
29. Liu, J. *et al.* Validation of MODIS albedo retrieval algorithm: Dependence of albedo on solar zenith angle. *Remote Sens. Environ.* **114,** 738–760 (2010).
30. Dee, D. P. *et al.* The ERA-interim reanalysis: Configuration and performance of the data assimilation system. *Q. J. R. Meteorol. Soc.* **137,** 553–597 (2011).
31. Mesinger, F. *et al.* North American regional analysis. *Bull. Am. Meteorol. Soc.* **87,** 343–360 (2006).

Acknowledgements

This study was supported by the startup financial support provided by the University at Albany, State University of New York and by the National Science Foundation (NSF IPA no. 0824354). The ECMWF interim reanalysis data is obtained from the ECMWF data server. The NARR reanalysis data is provided by the National Oceanic and Atmospheric Administration/National Centers for Environmental Prediction/Environmental Modeling Center.

Author contributions

L.Z. and Y.T. contributed the central idea, carried out data analyses, prepared the data and figures and wrote the initial draft of the paper. The remaining authors contributed to refining the ideas and to writing this paper.

Additional information

The authors declare no competing financial interests. Supplementary information accompanies this paper on www.nature.com/natureclimatechange. Reprints and permissions information is available online at www.nature.com/reprints. Correspondence and requests for materials should be addressed to L.Z.